ACS Combinatorial Science

pubs.acs.org/acscombsci

Research Article

# High Entropy and Sluggish Diffusion "Core" Effects in Senary FCC Al−Co−Cr−Fe−Ni−Mn Alloys

Abhishek Mehta* and Yongho Sohn

Cite This: *ACS Comb. Sci.* 2020, 22, 757−767

Read Online

ACCESS | Metrics & More | Article Recommendations | Supporting Information

**ABSTRACT:** Relative role of enthalpy and entropy in the stabilization of senary FCC Al−Co−Cr−Fe−Ni−Mn high entropy alloys was investigated via a high throughput combinatorial solid-to-solid diffusion couple approach. Many off-equiatomic compositions of FCC $Al_pCo_qCr_rFe_sNi_tMn_u$ were generated by the diffusing Al and Ni in equiatomic $Co_{20}Cr_{20}Fe_{20}Ni_{20}Mn_{20}$ alloy, i.e., the $Al_{48}Ni_{52}$ vs $Co_{20}Cr_{20}Fe_{20}Ni_{20}Mn_{20}$ diffusion couple, annealed at 900°, 1000°, 1100°, and 1200 °C. Above 1000 °C, the solubility limit of Al in off-equiatomic $Al_pCo_qCr_rFe_sNi_tMn_u$ alloy was determined to be higher than the solubility limit of Al in equiatomic $Al_xCoCrFeNiMn$ alloy. Compositions corresponding to the highest solubility limit of Al in off-equiatomic $Al_pCo_qCr_rFe_sNi_tMn_u$ alloy exhibited a lower free energy of mixing, i.e., higher thermodynamic stability, than equiatomic $Al_xCoCrFeNiMn$ compositions, at 1100 °C and above. Therefore, the role of enthalpy was estimated to be significant in achieving higher thermodynamic stability in off-equiatomic alloys, since they always have lower entropy of mixing than their equiatomic counterparts. The magnitude of interdiffusion coefficients of individual elements in Al−Co−Cr−Fe−Ni−Mn alloys were compared to the interdiffusion coefficients in relevant quinary, quaternary, and ternary solvent-based alloys. Interdiffusion coefficients were not necessarily lower in FCC Al−Co−Cr−Fe−Ni−Mn alloys; therefore no sluggish diffusion was observed in FCC HEA, but diffusion of individual elements in BCC Al−Co−Cr−Fe−Ni−Mn alloy followed the sluggish diffusion hypothesis except for Ni. All compositions in the FCC Al−Co−Cr−Fe−Ni−Mn alloy were observed to comply with existing empirical single phase formation rules in high entropy alloys.

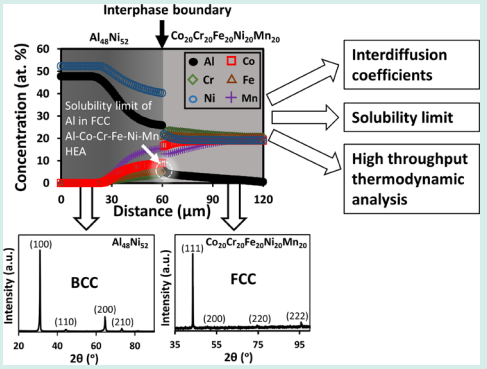


**KEYWORDS:** *high entropy alloys, enthalpy, entropy, interdiffusion, solubility, stability*



## INTRODUCTION

Brought to attention in 2004 was a novel class of materials named high entropy alloys (HEAs) that contain four or five principal elements in near-equiatomic concentration.[1,2] Design principle for HEAs is to achieve maximum configurational entropy of mixing, which would stabilize single phase solid solutions in comparison to low entropy intermetallic phases. However, many HEAs studied exhibit multiphase microstructure, and only a few HEAs were characterized as single-phase solid-solution.[3] The experimental observations of multiphase microstructure cast a doubt on the theory of entropic stabilization of a single phase in HEAs, and the suppression of second phase formation (i.e., intermetallics) may not occur in all HEAs even if entropy of mixing remains above the theoretical limit ($\geq 1.5R$). These findings were brought forth to question the validity of four initially proposed "core" effects: high entropy, sluggish diffusion, lattice distortion, and a cocktail effect,[4] which are considered the founding principles of HEAs.

Our previous work[5] on quinary Al−Co−Cr−Fe−Ni alloys had demonstrated that compositions with higher configurational entropy of mixing do not always correspond to higher thermodynamic stability when compared to compositions with lower configurational entropy of mixing. The role of enthalpy of mixing was observed to be more significant in alloys with a lower entropy of mixing than in alloy composition with a higher entropy of mixing. Zhang et al.[6] also suggested that the thermodynamic stability of HEAs cannot be governed alone by the entropy term because equiatomic composition does not always result in the lowest Gibbs free energy. Otto et al.[3] also investigated the quinary compositions of HEAs and suggested that a higher entropy of mixing will not always result in suppression of secondary phase formation based on thermodynamic stability criteria. Commonly reported in these studies is the significance of enthalpy contribution toward the overall thermodynamic stability of HEAs.

**Received:** May 20, 2020
**Revised:** August 29, 2020
**Published:** October 19, 2020




https://dx.doi.org/10.1021/acscombsci.0c00096
*ACS Comb. Sci.* 2020, 22, 757−767

The sluggish diffusion effect in HEAs postulates that diffusion of individual elements in alloys with higher configurational entropy of mixing should be slower than those with lower configurational entropy of mixing. On the contrary, a majority of the experimental work on the measurement of tracer diffusion coefficients in HEAs[7−14] suggested that diffusion is not sluggish in HEAs. Few review articles[15−17] also cast a doubt on the existence of sluggish diffusion in HEAs. Similarly, interdiffusion coefficients determined for HEAs also demonstrated that interdiffusion of individual elements may not always be slow in alloys with higher configurational entropy of mixing.[5,18,19]

Most of the studies to investigate the core effects had examined HEAs up to maximum of five components (i.e., quinary system). Therefore, in this study, two "core" effects, i.e., high entropy and sluggish diffusion effects, were examined in senary FCC Al−Co−Cr−Fe−Ni−Mn alloys using high throughput combinatorial solid-to-solid diffusion couple investigation, which allows simultaneous measurement of interdiffusion coefficients, determination of a solubility limit of individual elements, and examination of thermodynamic stability. Off-equiatomic senary compositions in $Al_pCo_qCr_rFe_sNi_tMn_u$ alloys were generated by isothermally annealing $\beta$-$Al_{48}Ni_{52}$ vs $Co_{20}Cr_{20}Fe_{20}Ni_{20}Mn_{20}$ diffusion couples in the temperature range from 900 to 1200 °C. Average effective interdiffusion coefficients and the solubility limit of Al in $Al_pCo_qCr_rFe_sNi_tMn_u$ alloy were determined as a function of temperature. Interdiffusion coefficients were compared with those of various elements in relevant, solvent-based ternary and quaternary alloys. The solubility limit of Al in off-equiatomic $Al_pCo_qCr_rFe_sNi_tMn_u$ was also compared with that in equiatomic high entropy $Al_xCoCrFeNiMn$ alloy. Results were analyzed with regard to the contributions from enthalpy ($\Delta H$) and entropy ($-T\Delta S$) to the thermodynamic stability ($\Delta G$) of equiatomic and off-equiatomic Al−Co−Cr−Fe−Ni−Mn alloys.

## EXPERIMENTAL PROCEDURES

The single-phase solid solutions of $\beta$-$Al_{48}Ni_{52}$ (B2) and FCC $Co_{20}Cr_{20}Fe_{20}Ni_{20}Mn_{20}$ (FCC) alloys were arc-melted using Al, Co, Cr, Fe, Ni, and Mn with a purity of 99.9% or higher. Alloys were arc-melted using the Centorr Arc melter under an Ar environment in a water-cooled Cu crucible. To ensure the compositional homogeneity, alloy ingots were melted, flipped, and remelted five times. As-cast ingots were then homogenized at 1100 °C for 48 h in a quartz-encapsulated argon atmosphere and subsequently water-quenched. Phase constituents (e.g, single phase formation) and microstructural homogeneity were examined with an Malvern Panalytical Empyrean X-ray diffraction system and Zeiss Ultra-55 field emission scanning electron microscope (FE-SEM) equipped with Thermo-Scientific X-ray energy dispersive spectroscopy (XEDS). The composition of the homogenized $Al_{48}Ni_{52}$ disc was measured to be 48.10 (±0.29) atom % Al and 51.90 (±0.34) atom % Ni. The composition of the homogenized $Co_{20}Cr_{20}Fe_{20}Ni_{20}Mn_{20}$ disc was measured to be 19.21 (±0.19) atom % Co, 20.59 (±0.26) atom % Cr, 20.14 (±0.24) atom % Fe, 19.18 (±0.17) atom % Ni, and 20.91 (±0.23) atom % Mn.

Homogenized alloys were sectioned into 3 mm discs using a low speed diamond saw and metallographically polished down to a 1 $\mu$m surface finish. Diffusion couples were fabricated by pressing the metallographically prepared surfaces of $\beta$-$Al_{48}Ni_{52}$ and $Co_{20}Cr_{20}Fe_{20}Ni_{20}Mn_{20}$ alloys against each other by using two stainless steel clamping jigs. Thin alumina spacers were placed between the alloy and stainless steel jig to avoid any interdiffusion between the alloys and jigs. The assembled diffusion couple along with a tantalum foil (i.e., oxygen getter) was placed in a quartz tube, evacuated to a pressure of $8.0 \times 10^{-6}$ Torr or better, and flushed alternately with high purity Ar and $H_2$ gas. The evacuation and flushing procedure was repeated several times before the quartz tube was sealed, creating a closed, high purity Ar atmosphere for the diffusion couples. More details on diffusion couple fabrication can be found elsewhere.[20−25] Each diffusion couple was isothermally annealed at 900, 1000, 1100, and 1200 °C for 240, 120, 48, and 24 h, respectively. After annealing, all diffusion couples were water quenched to preserve the high temperature microstructure. Then, each diffusion couple was mounted in cold resin epoxy, and its cross-section was metallographically polished down to a 1 $\mu$m surface finish. The microstructure of each diffusion couple was examined with a Zeiss Ultra-55 FE-SEM, equipped with a Thermo-Scientific XEDS. A minimum of three concentration profiles across the interdiffusion zone of each diffusion couple were obtained by point-to-point acquisition using XEDS equipped on SEM. XEDS data were converted to a concentration of various constituent elements in atom percent via standardless quantitative analysis.

A pseudobinary phase diagram between Al and equiatomic CoCrFeNiMn alloys (i.e., $Al_xCoCrFeNiMn$) was prepared using PANDAT software (CompuTherm LLC) for the calculation of a multicomponent phase diagram using the PanHEA thermodynamic database for high entropy alloys. The solubility limit of Al in the $Al_xCoCrFeNiMn$ alloy was directly determined using the FCC solvus line on the phase diagram as a function of temperature.

## RESULTS AND DISCUSSION

**High Entropy Effect in Senary Al−Co−Cr−Fe−Ni−Mn High Entropy Alloys.** The amount of Al in Al−Co−Cr−Fe−Ni−Mn alloy dictates the overall microstructure of the alloy. For instance, in as-cast $Al_xCoCrFeNiMn$ alloy, the FCC phase is stable for $x < 0.435$ (~8 atom % Al), the BCC phase is stable for $x > 1.25$ (~20 atom % Al), and both phases (i.e., FCC + BCC) are stable for $0.435 \leq x \leq 0.87$.[26] Therefore, a combinatorial diffusion couple approach was used to determine the solubility limit of Al in off-equiatomic FCC $Al_pCo_qCr_rFe_sNi_tMn_u$ alloys.

Figure 1 presents the concentration profiles superimposed on backscatter electron micrographs from the $Al_{48}Ni_{52}$ vs $Co_{20}Cr_{20}Fe_{20}Ni_{20}Mn_{20}$ diffusion couples isothermally annealed at (a) 900 °C for 240 h, (b) 1000 °C for 120 h, (c) 1100 °C for 48 h, and (d) 1200 °C for 24 h. From interdiffusion of Al and Ni from $\beta$-$Al_{48}Ni_{52}$ (B2) into the $Co_{20}Cr_{20}Fe_{20}Ni_{20}Mn_{20}$ (FCC) alloy, continuous off-equiatomic compositions of FCC $Al_pCo_qCr_rFe_sNi_tMn_u$ evolved; however, BCC or duplex phases were not observed in the starting microstructure of $Co_{20}Cr_{20}Fe_{20}Ni_{20}Mn_{20}$ alloy, similar to $Al_{48}Ni_{52}$ vs $Co_{25}Cr_{25}Fe_{25}Ni_{25}$ diffusion couples;[5] i.e., the $Al_pCo_qCr_rFe_sNi_tMn_u$ alloy remained a FCC single phase. At higher temperatures, Kirkendall pores were observed as dark spots near the interface shown in Figure 1c and d, on the $\beta$-$Al_{48}Ni_{52}$ (B2) side, which should be considered a BCC single phase, of the diffusion couple.

Figure 2a shows the pseudobinary phase diagram between Al and equiatomic CoCrFeNiMn alloys. The solubility limit of Al in $Al_xCoCrFeNiMn$ alloy was directly determined using the


https://dx.doi.org/10.1021/acscombsci.0c00096
ACS Comb. Sci. 2020, 22, 757−767

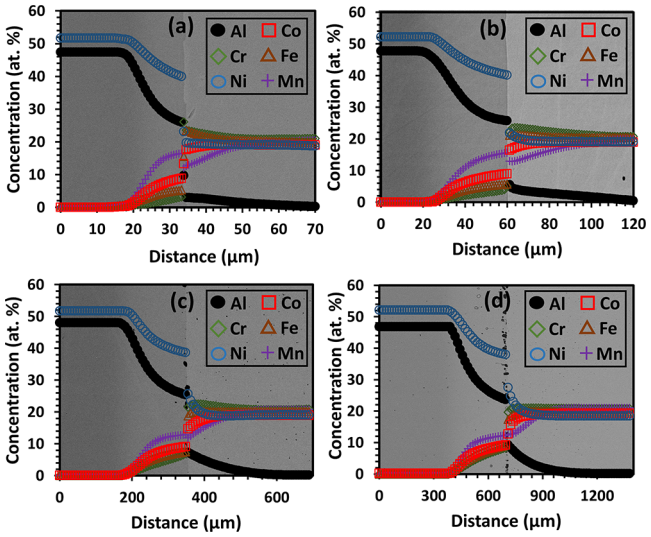


**Figure 1.** Concentration profiles superimposed on backscatter electron micrographs of $Al_{48}Ni_{52}$ vs $Co_{20}Cr_{20}Ni_{20}Fe_{20}Mn_{20}$ diffusion couples isothermally annealed at (a) 900 °C for 240 h, (b) 1000 °C for 120 h, (c) 1100 °C for 48 h, and (d) 1200 °C for 24 h.

FCC solvus line on the phase diagram. Figure 2b shows a relative comparison of the maximum solubility limit of Al in equiatomic FCC $Al_xCoCrFeNiMn$ alloy, determined from a calculated phase diagram, and the solubility limit of Al in off-equiatomic FCC $Al_pCo_qCr_rFe_sNi_tMn_u$ alloy, determined from diffusion couple experiments. The solubility limit reported in this work represents one of the infinite solubility limits (i.e., one of the end-point composition of the infinite tie-lines), and a large number of diffusion couple experiments with varying terminal alloy compositions would be required to map the entire solubility limit phase boundary. Also, a semi-infinite diffusion couple typically exhibits a unique diffusion path, which is difficult to determine a priori, but the solubility limit compositions generated in this work are justifiably close to the equiatomic compositions (with similar enthalpy and entropy contributions). A maximum solubility of Al in as-cast $Al_xCoCrFeNiMn$ (i.e., $x = 0.435$) alloy is also indicated in Figure 2b. Figure 2b delineates that the solubility limit of Al in $Al_pCo_qCr_rFe_sNi_tMn_u$ alloy at temperature above 1000 °C is higher than that in $Al_xCoCrFeNiMn$ alloy. The configurational entropy for the compositions corresponding to the maximum solubility limit of Al in $Al_pCo_qCr_rFe_sNi_tMn_u$ and $Al_xCoCrFeNiMn$ alloys is shown in Figure 2c. The configurational entropy of equiatomic $Al_xCoCrFeNiMn$ alloy is always higher than that of off-equiatomic $Al_pCo_qCr_rFe_sNi_tMn_u$ alloy for all temperatures. Therefore, the entropy of mixing plays a greater role in minimizing the overall free energy for stabilizing the single phase in equiatomic $Al_xCoCrFeNiMn$ alloy than in off-equiatomic $Al_pCo_qCr_rFe_sNi_tMn_u$ alloy, i.e., $|-T\Delta S_{mix}|^{equiatomic\text{-}alloy} > |-T\Delta S_{mix}|^{off\text{-}equiatomic\text{-}alloy}$.

Enthalpy of mixing ($\Delta H_{mix}$) is typically determined using the regular solution model:[27]

$$\Delta H_{mix} = \sum_{i=1}^{n-1} \sum_{j=i+1}^{n} (4 \times \Delta H_{ij}^{mix}) X_i X_j \quad (1)$$

where $\Delta H_{ij}^{mix}$ is the binary pair enthalpy of mixing between components, $i$ and $j$, which can be estimated using Miedema's macroscopic model for liquid binary alloy,[28,29] and $X_i$ is the

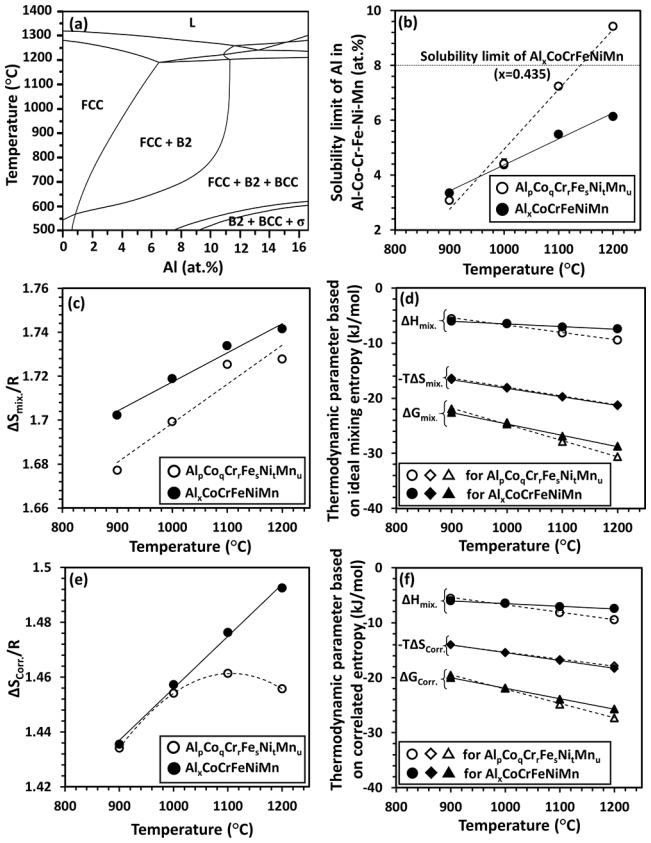


**Figure 2.** (a) Pseudobinary phase diagram of between Al and equiatomic CoCrFeNiMn. (b) Comparison of maximum solubility limit of Al as a function of temperature in FCC $Al_pCo_qCr_rFe_sNi_tMn_u$ and $Al_xCoCrFeNiMn$ alloys. (c) Mixing (i.e., Boltzmann) entropy as a function of temperature. (d) Thermodynamic stability parameters based on mixing entropy for off-equiatomic $Al_pCo_qCr_rFe_sNi_tMn_u$ and equiatomic $Al_xCoCrFeNiMn$ alloys. (e) Correlated configurational entropy as a function of temperature. (f) Correlated thermodynamic stability parameters for off-equiatomic $Al_pCo_qCr_rFe_sNi_tMn_u$ and equiatomic $Al_xCoCrFeNiMn$ alloys. In b–f, open symbols represent thermodynamic parameters for off-equiatomic $Al_pCo_qCr_rFe_sNi_tMn_u$ alloy, and filled symbols represent thermodynamic parameters for equiatomic $Al_xCoCrFeNiMn$ alloy.

mole fraction of component $i$. For the compositions corresponding to the maximum solubility limit of Al at 1100 °C and above, $\Delta H_{mix}$ has a larger contribution toward the free energy of mixing ($\Delta G_{mix}$) for the off-equiatomic $Al_pCo_qCr_rFe_sNi_tMn_u$ alloy than for the equiatomic $Al_xCoCrFeNiMn$ alloy, i.e., $|\Delta H_{mix}|^{off\text{-}equiatomic\text{-}alloy} > |\Delta H_{mix}|^{equiatomic\text{-}alloy}$. Figure 2d presents the thermodynamic stability parameters, i.e., $\Delta H_{mix}$, $-T\Delta S_{mix}$, and $\Delta G_{mix}$, as a function of temperature for the equiatomic $Al_xCoCrFeNiMn$ and off-equiatomic $Al_pCo_qCr_rFe_sNi_tMn_u$ alloys. At 1100 °C and above, $\Delta G_{mix}$ of $Al_pCo_qCr_rFe_sNi_tMn_u$ alloy is smaller than that of $Al_xCoCrFeNiMn$. In other words, at higher temperatures, alloys of off-equiatomic composition with a lower entropy of mixing can achieve higher thermodynamic stability than the alloys of equiatomic composition with a higher entropy of mixing. Moreover, the role of $\Delta H_{mix}$ is important in achieving the lower free energy more so in off-equiatomic alloys than in equiatomic alloys.

The correlation effect among constituent elements in HEAs would give rise to fluctuation in lattice potential energy mainly due to the atomic size mismatch and bond energy mismatch of


https://dx.doi.org/10.1021/acscombsci.0c00096
ACS Comb. Sci. 2020, 22, 757−767

neighboring atoms.[30] Normalized potential energy fluctuations ($p$) with respect to thermal energy ($\sim k_B T$) can be determined using[30,31]

$$p = 4.12\delta \times \sqrt{\frac{\bar{K}\bar{V}}{k_B T}} + 2\sqrt{\frac{\sqrt{\sum_i \sum_{j,i\neq j} X_i X_j (\Delta H_{ij}^{\mathrm{mix}} - \bar{H})^2}}{k_B T}} \quad (2)$$

where $\delta \left(=\sqrt{\sum_{i=1}^{n} X_i \left(1 - \frac{r_i}{\sum X_i r_i}\right)^2}\right)$ represents the mismatch in atomic size, $r_i$ is the atomic radius, $\bar{K}$ is the composition-weighted average bulk modulus, and $\bar{V}$ is the composition-weighted average atomic volume. This potential energy fluctuation would result in excess entropy ($S_E$) in HEAs, which can be mathematically expressed as[30,31]

$$S_E = R \times \left[1 + \frac{p}{2} - \ln(p) + \ln(1 - e^{-p}) - \frac{p}{2} \times \frac{1 + e^{-p}}{1 - e^{-p}}\right] \quad (3)$$

Correlated configurational entropy of mixing ($\Delta S_{\mathrm{corr}}$) can be expressed by the sum of ideal and excess entropy terms, i.e., $\Delta S_{\mathrm{corr}} = \Delta S_{\mathrm{mix}} + S_E$. Figure 2e presents the correlated configurational entropy ($\Delta S_{\mathrm{corr}}$) as a function of temperature for the compositions corresponding to the maximum solubility limit of Al in $Al_pCo_qCr_rFe_sNi_tMn_u$ and $Al_xCoCrFeNiMn$ alloys. Similar to mixing entropy, correlated configurational entropy of $Al_pCo_qCr_rFe_sNi_tMn_u$ is always lower than that of $Al_xCoCrFeNiMn$. The corresponding correlated free energy of mixing ($\Delta G_{\mathrm{corr}}$) is also lower for $Al_pCo_qCr_rFe_sNi_tMn_u$ than the $Al_xCoCrFeNiMn$ at a temperature of 1100 °C and above, as shown in Figure 2f. Therefore, $\Delta H_{\mathrm{mix}}$ plays an important role in achieving higher thermodynamic stability due to correlation effects in off-equiatomic $Al_pCo_qCr_rFe_sNi_tMn_u$ alloy more so than in an equiatomic $Al_xCoCrFeNiMn$ alloy. Indeed, entropy plays a major role in stabilizing a given HEA since $|-T\Delta S|/|\Delta H| \approx 2.5-3.5$; however, the role of $\Delta H_{\mathrm{mix}}$ may become important in achieving higher thermodynamic stability in off-equiatomic Al−Co−Cr−Fe−Ni−Mn alloy than in equiatomic alloy.

**Phase Stability in Al−Co−Cr−Fe−Ni−Mn.** The role of both enthalpy and entropy of the solid-solution phase is important in achieving the thermodynamic stability of a phase. However, for a given composition, it is also important to concurrently validate that there is no other competing ordered intermetallic (IM) phase that can achieve higher thermodynamic stability than the solid solution (SS) phase. Otherwise, the intermetallic phase would precipitate from the solid solution, accompanied by a change in composition of solid solution phase according to its solubility. The criteria for the suppression of precipitation of the ordered phases can be described as[17] $\Delta G_{SS} < \Delta G_{IM}$, i.e., $\Delta H_{\mathrm{mix}} - T\Delta S_{\mathrm{mix}} < \Delta H_{IM} - T\Delta S_{IM}$. The enthalpy of mixing for an intermetallic phase can be determined using[32]

$$\Delta H_{IM} = \sum_{i=1}^{n-1} \sum_{j=i+1}^{n} (4 \times \Delta H_{ij}^{IM}) X_i X_j \quad (4)$$

where $\Delta H_{ij}^{IM}$ represents the binary pair enthalpy of formation of the most stable intermetallic compound between $i$ and $j$. The $\Delta H_{ij}^{IM}$ can be adopted from density-functional-theory (DFT) calculations.[33] The $\Delta S_{IM}$ is a function of $\Delta S_{\mathrm{mix}}$ and typically correlated by the structural ordering related parameter ($\kappa_2$) as $\Delta S_{IM} = \kappa_2 \Delta S_{\mathrm{mix}}$[32] The $\kappa_2$ parameter can be estimated by the site occupancy in the sublattice model of the intermetallic phase. The value of $\kappa_2$ varies between 0 and 1; however, $\kappa_2$ is more than 0.4 for $L1_2$ or B2 crystal symmetry and increases with a decrease in level of ordering. Senkov and Miracle[32] have applied the value of $\kappa_2 = 0.6$ to $Al_{0.25}CoCrFeNi$ and predicted the splitting of single phase fcc solid solution at 1000 °C, but a stable fcc solid solution was observed experimentally. A small change, $\kappa_2 \leq 0.5$, correctly predicts the phase stability in $Al_{0.25}CoCrFeNi$ alloy. Therefore, by assuming $\kappa_2 = 0.45$ ($\kappa_2$ decrease with an increase in ordering), free energy of solid solution ($\Delta G_{SS}^{AlCoCrFeNiMn}$) and ordered ($\Delta G_{IM}^{AlCoCrFeNiMn}$) phase in equiatomic AlCoCrFeNiMn alloy can be estimated as −33.8 kJ/mol and −37.1 kJ/mol, respectively, at 1200 °C. This indicates that an intermetallic phase would be more stable than a solid solution phase, and therefore, the equiatomic alloy composition would result in precipitation of an ordered intermetallic phase, as was experimentally observed.[26] However, the solid solution compositions examined in this work, corresponding to the maximum solid-solubility limit of Al at respective temperatures, were observed to be more stable than their competing ordered intermetallic phase, as illustrated in Table 1.

**Table 1. Comparison of Free Energy of Mixing of Solid Solution and Intermetallic Phases Examined in This Work**

| | $Al_xCoCrFeNiMn$ (from phase diagram) | | $Al_pCo_qCr_rFe_sNi_tMn_u$ (from diffusion couple) | |
|---|---|---|---|---|
| temperature (°C) | $\Delta G_{SS}$ (kJ/mol) | $\Delta G_{IM}$ (kJ/mol) | $\Delta G_{SS}$ (kJ/mol) | $\Delta G_{IM}$ (kJ/mol) |
| 900 | −22.6 | −19.1 | −21.9 | −18.1 |
| 1000 | −24.7 | −21.2 | −24.4 | −20.9 |
| 1100 | −26.9 | −23.4 | −27.8 | −25.9 |
| 1200 | −28.7 | −25.0 | −30.6 | −30.0 |

**Role of Enthalpy of Mixing.** A high entropy effect postulates that equiatomic alloys with random solid-solution microstructure have the highest entropy of mixing and consequently exhibit the highest thermodynamic stability at high temperatures. Generally for transition metal HEAs, $|-T\Delta S_{\mathrm{mix}}| > |\Delta H_{\mathrm{mix}}|$; therefore, entropic contribution is more significant at higher temperatures than enthalpy contribution toward the stability ($\Delta G_{\mathrm{mix}}$). This is referred to as *entropic stabilization* of an alloy, which is typically accomplished with a minimum of four components in equal amounts. However, the role of enthalpy is typically not addressed when comparing HEAs with similar constituent elements with varying compositions, since the composition corresponding to the highest configurational entropy is presumed to be more stable than the compositions corresponding to the lower entropy.

Compositions for off-equiatomic FCC Al−Co−Cr−Fe−Ni[5] and Al−Co−Cr−Fe−Ni−Mn alloys, corresponding to the highest solubility limit for Al, were observed to exhibit higher thermodynamic stability than equiatomic composition at temperatures of 1100 °C and above. In these alloys, the entropy of mixing always plays a vital role in stabilizing the single phase; however, the role of enthalpy of mixing cannot be


https://dx.doi.org/10.1021/acscombsci.0c00096
ACS Comb. Sci. 2020, 22, 757−767

**Table 2. Binary Enthalpy of Mixing Calculated by Miedema's Model[28,29] for Atomic Pair between Elements *i* and *j* in Various Co−Cr−Fe−Ni Based Alloy Systems[33]**

| alloy systems | | | | | | | |
|---|---|---|---|---|---|---|---|
| AlCoCrFeNiMn | | AlCoCrFeNi | | CoCrFeNiMn | | CoCrFeNiCu | |
| binary pairs ($i$–$j$) | $\Delta H_{i-j}^{mix}$ (kJ/mol) | binary pairs ($i$–$j$) | $\Delta H_{i-j}^{mix}$ (kJ/mol) | binary pairs ($i$–$j$) | $\Delta H_{i-j}^{mix}$ (kJ/mol) | binary pairs ($i$–$j$) | $\Delta H_{i-j}^{mix}$ (kJ/mol) |
| Al−Co | −19 | Al−Co | −19 | Mn−Co | −5 | Cu−Co | 6 |
| Al−Cr | −10 | Al−Cr | −10 | Mn−Cr | 2 | Cu−Cr | 12 |
| Al−Fe | −11 | Al−Fe | −11 | Mn−Fe | 0 | Cu−Fe | 13 |
| Al−Ni | −22 | Al−Ni | −22 | Mn−Ni | −8 | Cu−Ni | 4 |
| Al−Mn | −19 | Co−Cr | −4 | Co−Cr | −4 | Co−Cr | −4 |
| Mn−Co | −5 | Co−Fe | −1 | Co−Fe | −1 | Co−Fe | −1 |
| Mn−Cr | 2 | Co−Ni | 0 | Co−Ni | 0 | Co−Ni | 0 |
| Mn−Fe | 0 | Cr−Fe | −1 | Cr−Fe | −1 | Cr−Fe | −1 |
| Mn−Ni | −8 | Cr−Ni | −7 | Cr−Ni | −7 | Cr−Ni | −7 |
| Co−Cr | −4 | Fe−Ni | −2 | Fe−Ni | −2 | Fe−Ni | −2 |
| Co−Fe | −1 | | | | | | |
| Co−Ni | 0 | | | | | | |
| Cr−Fe | −1 | | | | | | |
| Cr−Ni | −7 | | | | | | |
| Fe−Ni | −2 | | | | | | |

**Table 3. Compositions of Various Alloys Corresponding to the Maximum Solubility Limit of Al**

| | | maximum solubility limit of Al in atom % (values in parentheses are standard deviation in atom %) | | | | | |
|---|---|---|---|---|---|---|---|
| alloy system | $T$ (°C) | Al | Cr | Mn | Fe | Co | Ni |
| $Al_pCo_qCr_rFe_sNi_tMn_u$ [present work] | 900 | 3.07 (0.02) | 23.21 (0.34) | 12.86 (0.14) | 23.47 (0.04) | 17.95 (0.27) | 19.50 (0.16) |
| | 1000 | 4.39 (0.17) | 23.09 (0.23) | 12.78 (0.17) | 21.36 (0.35) | 16.79 (0.12) | 21.65 (0.48) |
| | 1100 | 7.24 (0.12) | 21.67 (0.18) | 12.40 (0.34) | 18.84 (0.06) | 14.97 (0.19) | 24.93 (0.37) |
| | 1200 | 9.42 (0.12) | 19.43 (0.14) | 12.48 (0.13) | 17.12 (0.23) | 13.25 (0.46) | 28.30 (0.19) |
| $Al_xCoCrFeNiMn$ [present work] | 900 | 3.35 | 19.33 | 19.33 | 19.33 | 19.33 | 19.33 |
| | 1000 | 4.38 | 19.124 | 19.124 | 19.124 | 19.124 | 19.124 |
| | 1100 | 5.49 | 18.90 | 18.902 | 18.90 | 18.90 | 18.90 |
| | 1200 | 6.14 | 18.77 | 18.77 | 18.77 | 18.77 | 18.77 |
| $Al_pCo_qCr_rFe_sNi_t$[5] | 900 | 4.08 (0.46) | 25.83 (0.16) | | 24.86 (0.24) | 22.25 (0.08) | 22.98 (0.32) |
| | 1000 | 5.48 (0.29) | 25.44 (0.21) | | 23.86 (0.19) | 20.91 (0.10) | 24.30 (0.23) |
| | 1100 | 8.57 (0.25) | 25.19 (0.13) | | 20.72 (0.23) | 17.65 (0.12) | 27.85 (0.17) |
| | 1200 | 10.42 (0.27) | 23.15 (0.37) | | 20.01 (0.14) | 15.99 (0.15) | 30.44 (0.15) |
| $Al_xCoCrFeNi$[5] | 900 | 5.34 | 23.67 | | 23.67 | 23.67 | 23.67 |
| | 1000 | 6.60 | 23.35 | | 23.35 | 23.35 | 23.35 |
| | 1100 | 7.93 | 23.02 | | 23.02 | 23.02 | 23.02 |
| | 1200 | 9.35 | 22.66 | | 22.66 | 22.66 | 22.66 |

neglected, because off-equiatomic alloy (i.e., lower entropy) compositions had higher thermodynamic stability than equiatomic alloy (i.e., higher entropy) compositions. Therefore, it is also important to simultaneously account for the enthalpy contribution along with entropy toward the overall thermodynamic stability, which has been also suggested in previous studies.[3,5,6,17,32]

At higher temperatures, the presence of Al may be an important factor for both off-equiatomic FCC Al−Co−Cr−Fe−Ni[5] and Al−Co−Cr−Fe−Ni−Mn alloys in accomplishing higher thermodynamic stability than their equiatomic counterparts, because of the strong negative binary interaction of Al with other elements. Binary pair enthalpy of mixing of Al ($\Delta H_{Al-X}^{mix}$) with each element (e.g, Co, Cr, Fe, Ni or Mn) is strongly negative in comparison to $\Delta H_{i-j}^{mix}$ values for other binary pair constituent elements in both Al−Co−Cr−Fe−Ni and Al−Co−Cr−Fe−Ni−Mn systems, as reported in Table 2. Therefore, as the solubility limit of Al in off-equiatomic $Al_pCo_qCr_rFe_sNi_tMn_u$ alloy increases with an increase in temperature, molar contribution of negative $\Delta H_{Al-X}^{mix}$ (X = Co, Cr, Fe, Ni, Mn) toward the overall $\Delta H_{mix}$ increases with increasing temperature. This is also true for equiatomic $Al_xCoCrFeNiMn$ alloy, but there exists a crossover between 1000 and 1100 °C when enthalpy contribution toward overall thermodynamic stability ($\Delta G_{mix}$) is higher for off-equiatomic compositions.

Variation in the solubility limit of other constituent elements as a function of temperature may be a possible reason for the existence of this cross over. Table 3 compares the variation in solubility limit for all elements in off-equiatomic, FCC $Al_pCo_qCr_rFe_sNi_tMn_u$ alloy. With an increase in temperature, the solubility limit of Ni and Al increases, while that of Co, Cr, and Fe decreases. Mn solubility remains nearly constant as a function of temperature. This variation of the solubility limit is also true for off-equiatomic $Al_pCo_qCr_rFe_sNi_t$ alloy measured using $Al_{48}Ni_{52}$ vs $Co_{25}Cr_{25}Fe_{25}Ni_{25}$ diffusion couples,[5] which is also reported in Table 3. However, in equiatomic $Al_xCoCrFeNi$ and $Al_xCoCrFeNiMn$ alloys, the solubility limit of Al increased with an increase in temperature, while others (i.e., Co, Cr, Fe, Ni, Mn) decreased, in order to maintain


https://dx.doi.org/10.1021/acscombsci.0c00096
ACS Comb. Sci. 2020, 22, 757−767

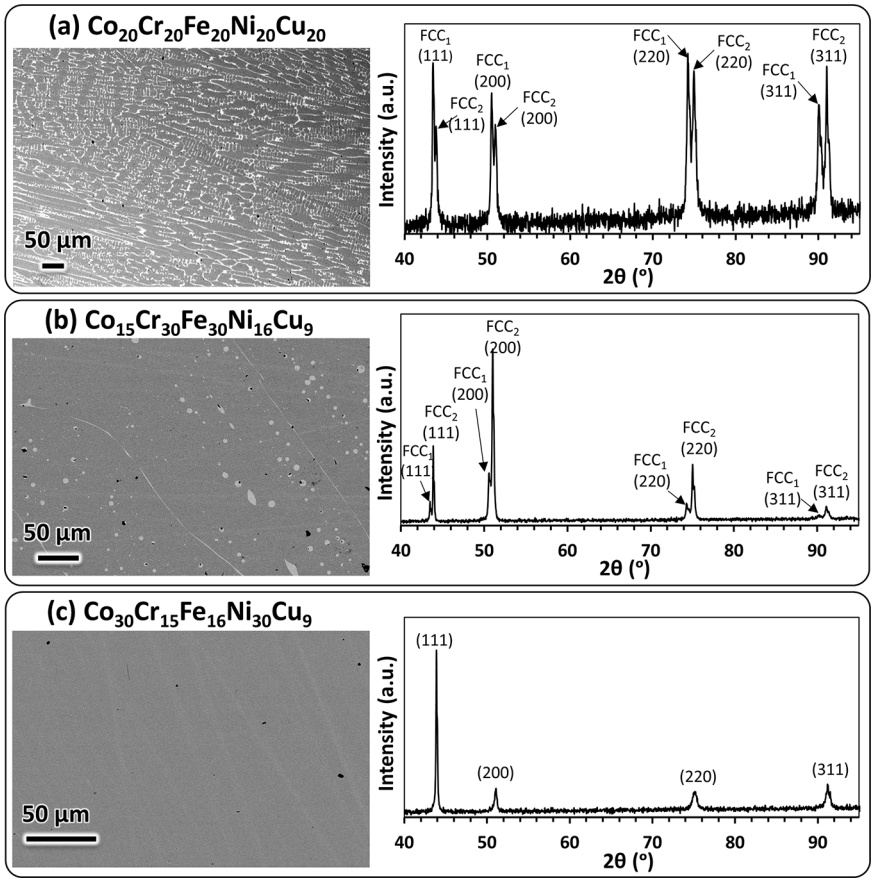


**Figure 3.** Representative backscatter electron micrograph and X-ray diffraction pattern of (a) $Co_{20}Cr_{20}Fe_{20}Ni_{20}Cu_{20}$, (b) $Co_{15}Cr_{30}Fe_{30}Ni_{16}Cu_9$, and (c) $Co_{30}Cr_{15}Fe_{16}Ni_{30}Cu_9$ alloys.

equiatomic composition. As reported in Table 2, $\Delta H^{mix}_{Al-Ni}$ is the lowest (−22 kJ/mol) among all binary pairs and would dictate the magnitude of overall enthalpy of mixing at higher temperatures due to an increase in solubility limit of Al and Ni. At 1100 °C and above, a larger magnitude in enthalpy of mixing, $|\Delta H_{mix}|$, for off-equiatomic alloys would result in overall higher thermodynamic stability than for equiatomic alloys. Both Al and Ni exhibit a negative binary pair enthalpy of mixing (i.e., $\Delta H^{mix}_{Al-X}$ or $\Delta H^{mix}_{Ni-X}$) with other elements, which would further lower the overall enthalpy of mixing in off-equiatomic alloy composition, in comparison to equiatomic composition.

Binary pair enthalpy of mixing ($\Delta H^{mix}_{ij}$) can provide an approximate estimate, whether the addition of new element would dissolve into the existing solid solution, i.e., a single phase alloy. Equiatomic CoCrFeNi is a single phase HEA.[34] If an additional alloying element has a significant, negative enthalpy of mixing with any of the four existing components, the overall alloy composition would have a tendency to precipitate a second phase (e.g, intermetallic compound or second phase). On the other hand, if an additional alloying element has a significant, positive enthalpy of mixing among all binary pairs, then the phase separation (i.e., miscibility gap) tendency would dominate. Table 2 also compares the binary pair enthalpy of mixing calculated using Miedema's model for Al−Co−Cr−Fe−Ni−Mn, Al−Co−Cr−Fe−Ni, Co−Cr−Fe−Ni−Mn, and Co−Cr−Fe−Ni−Cu alloys. It is evident from Table 2 and previous studies[26,35,36] that the addition of Al to equiatomic CoCrFeNi or CoCrFeNiMn beyond the solubility limit would lead to the formation of a second phase, while the addition of Cu would result in phase separation leading to the formation of two FCC phases.[37] The $\Delta H^{mix}_{Cu-X}$ (X = Co, Cr, Fe, Ni) is positive, and therefore the addition of Cu in a significant amount may potentially result in phase separation in Co−Cr−Fe−Ni−Cu alloy.

In order to validate the effect of Cu addition to single phase CoCrFeNi alloys, three additional alloys compositions of Co−Cr−Fe−Ni-Cu alloys, i.e., $Co_{20}Cr_{20}Fe_{20}Ni_{20}Cu_{20}$, $Co_{15}Cr_{30}Fe_{30}Ni_{16}Cu_9$, and $Co_{30}Cr_{15}Fe_{16}Ni_{30}Cu_9$, were fabricated via arc-melting and subsequently homogenized at 1100 °C for 48 h. The $\Delta H^{mix}_{Cu-Cr}$ and $\Delta H^{mix}_{Cu-Fe}$ have a high magnitude, and so $Co_{20}Cr_{20}Fe_{20}Ni_{20}Cu_{20}$ was cast as an equiatomic composition, while in the other compositions, $Co_{15}Cr_{30}Fe_{30}Ni_{16}Cu_9$ and $Co_{30}Cr_{15}Fe_{16}Ni_{30}Cu_9$, the amounts of Cr and Fe were kept at maximum and minimum by keeping the Cu constant at 9 atom %. Figure 3 presents representative backscatter electron micrographs and X-ray diffraction patterns from these three alloys. The $Co_{20}Cr_{20}Fe_{20}Ni_{20}Cu_{20}$ alloy with maximum Cu content exhibited the maximum phase separation. The $Co_{15}Cr_{30}Fe_{30}Ni_{16}Cu_9$ alloy with higher Cr and Fe contents exhibited a lower phase separation tendency due to relatively lower Cu content, while the $Co_{30}Cr_{15}Fe_{16}Ni_{30}Cu_9$ alloy with the lowest amount of Cu, Cr, and Fe exhibited no phase separation. It should be noted that the overall $\Delta H_{mix}$ in these three alloys was determined to be 3.2, 0.2664, and −0.1752 kJ/mol, respectively, which is in compliance with the solid solution phase formation rules given by Guo et al.[38] In this and previous studies,[39,40] the equiatomic


https://dx.doi.org/10.1021/acscombsci.0c00096
ACS Comb. Sci. 2020, 22, 757−767

$Co_{20}Cr_{20}Fe_{20}Ni_{20}Cu_{20}$ alloy has been reported to exhibit a microstructure consisting of two FCC phases, however the existing single phase formation rule fails to distinguish the phase separation tendency for this alloy.

Addition of Mn with the moderate binary pair enthalpy of mixing with other elements (i.e., Co, Cr, Fe, Ni) maintained the overall single phase solid solution microstructure in near equiatomic composition of CoCrFeNiMn alloy,[34] as shown by the terminal alloy ($Co_{20}Cr_{20}Fe_{20}Ni_{20}Mn_{20}$) of all diffusion couples in the present work.

The stability of the solid solution is often referred to as the ability of maximization for *random mixing* (i.e., state of maximum randomness). The formation of random solid solution would be mathematically attributed to the state of maximum configurational entropy of mixing, which would always be higher for the equiatomic compositions than the off-equiatomic compositions in the case of ideal solid solutions ($\Delta H_{mix} = 0$). Furthermore, in an ideal solid solution, the state of maximum randomness will correspondingly have the lowest free energy of mixing. However, Al−Co−Cr−Fe−Ni and Al−Co−Cr−Fe−Ni−Mn HEAs are nonideal solid solutions ($\Delta H_{mix} \neq 0$). Therefore, although the equiatomic composition would exhibit a higher randomness than for off-equiatomic composition, it will not necessarily exhibit the lowest free energy of mixing (i.e., maximum stability). This scenario is schematically presented in Figure 4, wherein the solid solution

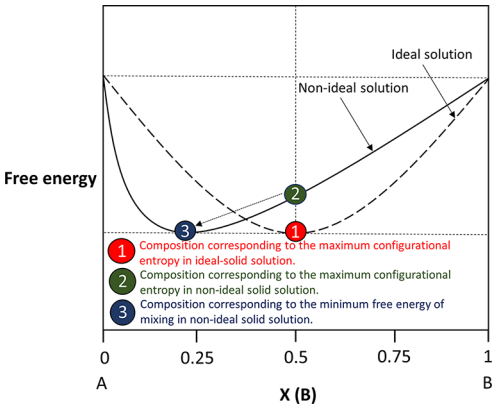


**Figure 4.** Free energy as a function of composition for equiatomic and off-equiatomic compositions in ideal and nonideal solid solution in a hypothetical binary system.

composition 2 would have the higher randomness (i.e., maximum configurational entropy), but solid solution composition 3 would have the higher thermodynamic stability. It should be noted that both the compositions (i.e., compositions 2 and 3 in Figure 4) will exhibit a stable solid solution microstructure at their respective composition, because no other phase will lie below the tangent at any composition of the free energy curve. However, relative stability (i.e., free energy of mixing) would be different for each composition. In such cases, enthalpy contribution would be important in lowering the overall free energy of mixing within solid solution phase when off-equiatomic composition has lower free energy than equiatomic composition.

It is worth mentioning that a substantial addition of Al in $Al_x$CoCrFeNi ($x > 0.88$) or $Al_x$CoCrFeNiMn ($x > 1.25$) alloys would yield the BCC structure, which had been attributed to an increase in lattice distortion due to the large atomic radius of Al.[41] However, second phase BCC precipitates still existed in the BCC matrix of $Al_x$CoCrFeNi ($x > 0.88$).[42]

**Interdiffusion Coefficients.** In addition to the solubility limit of Al, the average effective interdiffusion coefficients ($\overline{\overline{D}}_i^{eff}$), activation energy, and pre-exponential factors for Al, Co, Cr, Fe, Ni, and Mn were determined on the $\beta$-$Al_{48}Ni_{52}$ and $Co_{20}Cr_{20}Fe_{20}Ni_{20}Mn_{20}$ alloy side. The average effective interdiffusion coefficient can be determined for any component over a desired composition range by[43]

$$\int_{x_1}^{x_2} \tilde{J}_i \, dx = -\overline{\overline{D}}_i^{eff} (C_i(x_1) - C_i(x_2)) = -\frac{1}{2t} \int_{C_i(x_1)}^{C_i(x_2)} (x - x_o)^2 \, dC_i \quad (i = 1, 2..., n) \tag{5}$$

where, $\overline{\overline{D}}_i^{eff}$ represents the average effective interdiffusion coefficient of component $i$ for the composition range from $C_i(x_1)$ to $C_i(x_2)$. In this work, a full matrix of interdiffusion coefficients was not determined due to the limitation in obtaining the common intersection composition from the diffusion paths of five different diffusion couples in six dimensional composition space. Details of the procedure for the determination of average effective interdiffusion coefficients and limitations of using the Boltzmann−Matano method extended to a multicomponent system to determine the main and cross interdiffusion coefficients have been documented previously by Mehta and Sohn.[5]

Near the $Al_{48}Ni_{52}/Co_{20}Cr_{20}Fe_{20}Ni_{20}Mn_{20}$ interphase boundary, Kirkendall voids were observed on the $\beta$-$Al_{48}Ni_{52}$ side, similar to the $Al_{48}Ni_{52}/Co_{25}Cr_{25}Fe_{25}Ni_{25}$ interface in $Al_{48}Ni_{52}$ vs $Co_{25}Cr_{25}Fe_{25}Ni_{25}$ diffusion couples.[5] Figure 5 compares the $\overline{\overline{D}}_i^{eff}$ of Al, Co, Cr, Fe, Ni, and Mn, determined on the $\beta$-$Al_{48}Ni_{52}$ and $Co_{20}Cr_{20}Fe_{20}Ni_{20}Mn_{20}$ terminal alloy sides of the diffusion couples. The $\overline{\overline{D}}_i^{eff}$, activation energies and pre-exponential factors for Al, Co, Cr, Fe, Ni, and Mn determined from each diffusion couple are numerically reported in the Supporting Information (Table S1). Figure 6 compares the interdiffusion coefficients of Co, Cr, Fe, and Al in FCC $Al_pCo_qCr_rFe_sNi_tMn_u$ (via $Al_{48}Ni_{52}$ vs $Co_{20}Cr_{20}Fe_{20}Ni_{20}Mn_{20}$ diffusion couple) and $Al_pCo_qCr_rFe_sNi_t$ (via $Al_{48}Ni_{52}$ vs $Co_{25}Cr_{25}Fe_{25}Ni_{25}$ diffusion couple[5]), where only positive values of average effective interdiffusion coefficients are reported. The $\overline{\overline{D}}_i^{eff}$ of Cr and Al is higher in senary $Al_pCo_qCr_rFe_sNi_tMn_u$ alloy than in quinary $Al_pCo_qCr_rFe_sNi_t$ alloy. Figure 7 compares the coefficients for Co, Cr, Fe, Ni, and Al in BCC $Al_pCo_qCr_rFe_sNi_tMn_u$ and $Al_pCo_qCr_rFe_sNi_t$. A sluggish diffusion effect is largely followed by elements diffusing in BCC alloy as interdiffusion of Co, Cr, Fe, and Al is faster in quinary $Al_pCo_qCr_rFe_sNi_t$ alloy than in senary $Al_pCo_qCr_rFe_sNi_tMn_u$ alloy, except for Ni. An additional comparison of interdiffusion coefficients of individual elements in Fe−Cr−Ni,[44] Co−Cr−Fe−Ni,[45] Co−Cr−Fe−Ni−Mn,[46] Al−Co−Cr−Fe−Ni,[5] and Al−Co−Cr−Fe−Ni−Mn is presented in the Supporting Information (i.e., Table S2 and Table S3). Table S2 in the Supporting Information compares the $\overline{\overline{D}}_i^{eff}$ for Co, Cr, Fe, and Ni at 1000 °C in quaternary Co−Cr−Fe−Ni,[45] quinary Co−Cr−Fe−Ni−Mn,[46] quinary Al−Co−Cr−Fe−Ni,[5] and senary Al−Co−Cr−Fe−Ni−Mn systems. Interdiffusion diffusion coefficients of Cr in senary Al−Co−Cr−Fe−Ni−Mn alloy are larger than those in quaternary Co−Cr−Fe−Ni, quinary Co−Cr−Fe−Ni−Mn, and Al−Co−Cr−Fe−


https://dx.doi.org/10.1021/acscombsci.0c00096
ACS Comb. Sci. 2020, 22, 757−767

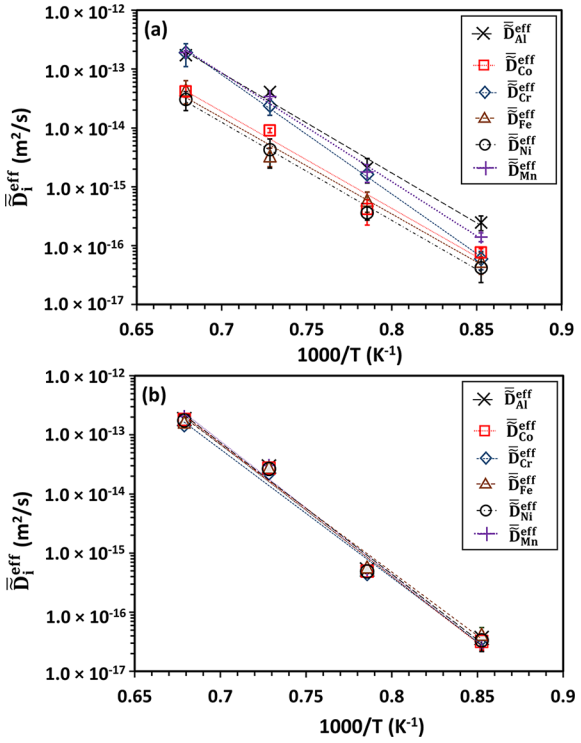


**Figure 5.** (a) Temperature dependence of average effective interdiffusion coefficients ($\overline{\overline{D}}_i^{eff}$) of Al, Co, Cr, Fe, Ni, and Mn in (a) FCC Al−Co−Cr−Fe−Ni−Mn (starting composition: $Co_{20}Cr_{20}Ni_{20}Fe_{20}Mn_{20}$) and BCC Al−Co−Cr−Fe−Ni−Mn (starting composition: $Al_{48}Ni_{52}$) alloys.

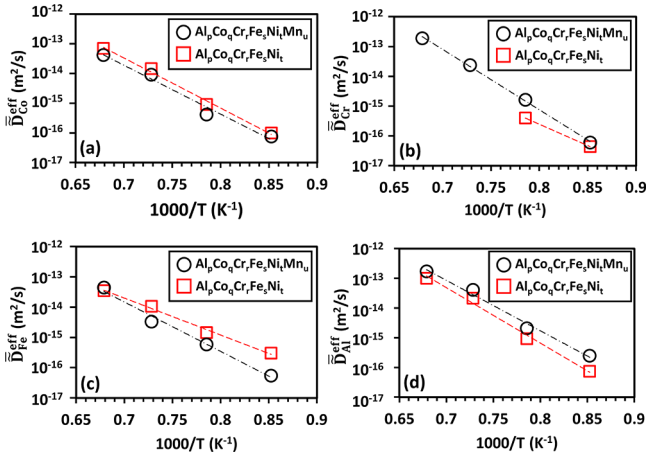


**Figure 6.** Comparison of average effective interdiffusion coefficients of (a) Co, (b) Cr, (c) Fe, and (d) Al in FCC Al−Co−Cr−Fe−Ni−Mn and Al−Co−Cr−Fe−Ni alloy.

Ni systems. Interdiffusion of Co is the fastest in the Al−Co−Cr−Fe−Ni system, and Ni exhibited the slowest interdiffusion in the quaternary Co−Cr−Fe−Ni system. In addition, Table S3 in the Supporting Information compares the $\overline{\overline{D}}_i^{eff}$s for Fe, Cr, and Ni in the FCC Fe−Cr−Ni alloy[44] with those in Al−Co−Cr−Fe−Ni and Al−Co−Cr−Fe−Ni−Mn alloys at 1100 °C. The interdiffusion coefficient of Cr is the largest in the senary Al−Co−Cr−Fe−Ni−Mn alloy, and therefore, the interdiffusion coefficient of a particular element may not necessarily decrease with an increase in the number of alloying elements in alloys with a higher entropy of mixing.

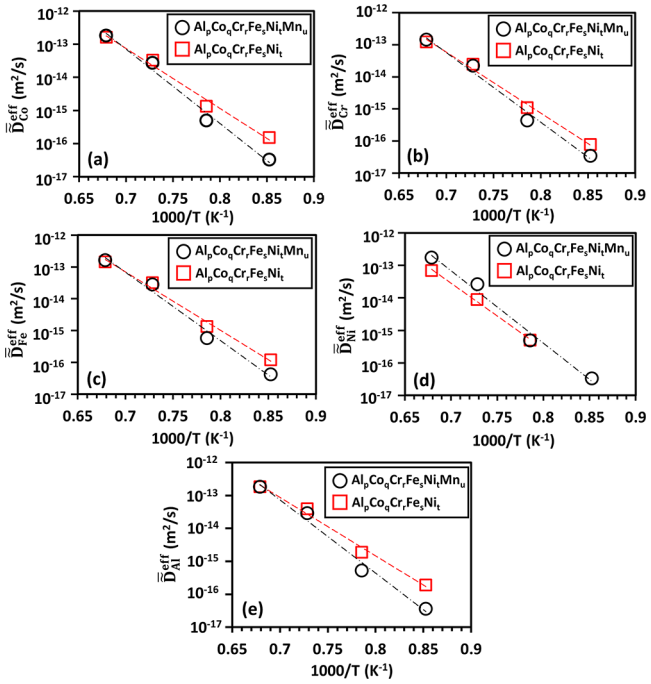


**Figure 7.** Comparison of average effective interdiffusion coefficients of (a) Co, (b) Cr, (c) Fe, (d) Ni, and (e) Al in BCC Al−Co−Cr−Fe−Ni−Mn and Al−Co−Cr−Fe−Ni alloy.

In an HEA, potential energy fluctuations in the lattice site have been correlated to the diffusivity of an element to justify the sluggish diffusion effect.[7] A larger variation in the lattice potential energy of atomic sites would result in anomalously slow diffusion due to creation of highly stable low energy sites (i.e., atomic traps). To that end, normalized potential energy fluctuation ($p$) was calculated for FeCrNi, CoCrFeNi, CoCrFeNiMn, $Al_{0.45}$CoCrFeNi, and $Al_{0.435}$CoCrFeNiMn alloys using a potential energy fluctuation (PEF) model,[30,31] given by eq 2. Temperature dependences of normalized PEF ($p$) in ternary FeCrNi, quaternary CoCrFeNi, quinary CoCrFeNiMn, $Al_{0.45}$CoCrFeNi, and senary $Al_{0.435}$CoCrFeNiMn alloys are presented in Figure 8. Normalized PEF ($p$) in general decreased with an increase in temperature and varied for different alloys as $p$(FeCrNi) ≈ $p$(CoCrFeNi) < $p$(CoCrFeNiMn) < $p$($Al_{0.45}$CoCrFeNiMn) <

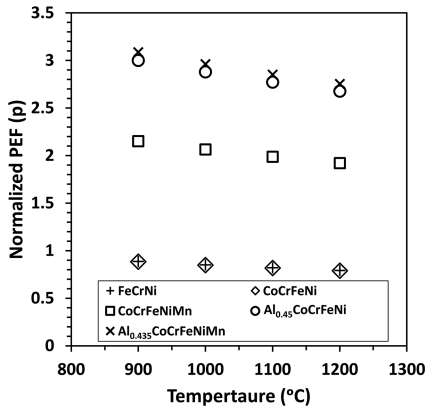


**Figure 8.** Temperature dependence of normalized potential energy fluctuation (PEF) in FeCrNi, CoCrFeNi, CoCrFeNiMn, $Al_{0.45}$CoCrFeNi, and $Al_{0.435}$CoCrFeNiMn alloys.


https://dx.doi.org/10.1021/acscombsci.0c00096
ACS Comb. Sci. 2020, 22, 757−767

$p(Al_{0.435}CoCrFeNiMn)$. The "sluggish diffusion" postulation then should be reflected by the diffusivity of individual elements in the opposite trend. However, a comparison of interdiffusion coefficients at various temperatures, as reported in Figure 6, Figure 7, Table S2 (Supporting Information), and Table S3 (Supporting Information) demonstrated that interdiffusion coefficients are not lower for all elements with higher PEF. This implies that potential energy fluctuations cannot always be correlated to the diffusivity in an alloy system, and therefore, a component in HEA with higher PEF may not always have a lower interdiffusion coefficient.

The magnitude of normalized PEF provides an idea for the characteristic of an atomic site, i.e., whether an atomic site will be trap or not, but it does not give any information on the *number of atomic trapping sites*. Diffusion will only become sluggish if the number of trapping sites is high. Ideally, in a vacancy exchange diffusion mechanism, *trapping of vacancies* is more important than *trapping of atoms* in low energy sites (i.e., atomic traps). Trapping a few atoms in an alloy system would not significantly slow down the diffusion.

**Phase Formation Rules.** Off-equiatomic $Al_pCo_qCr_rFe_sNi_tMn_u$ compositions generated on the FCC side of the diffusion couple in this study were subjected to generic phase formation rules for multicomponent alloys, which predict the ability of an alloy to form a solid solution. Predictor parameters such as $\Omega$,[47] $\delta$,[48] $\Delta H_{mix}$,[27] VEC,[49] and $\Delta\chi$[48] are typically employed to predict the formation of a solid solution phase in HEAs. The $\Omega$ term $(= T\Delta S_{mix}/|\Delta H_{mix}|)$ represents the relative effects of enthalpy and entropy of mixing in HEA. The $\delta$ is the atomic size mismatch. VEC represents the valence electron concentration that can be determined as a composition-weighted average VEC value from the constituent elements (i.e., $\sum X_i(\mathrm{VEC})_i$). The $\Delta\chi$ parameter $\left(= \sqrt{\sum_{i=1}^{n} X_i(\chi_i - \sum X_i\chi_i)^2}\right)$ is the electronegativity difference between constituent elements in HEA.

Figure 9 shows the solid-solubility predictors for various off-equiatomic FCC $Al_pCo_qCr_rFe_sNi_tMn_u$ compositions plotted as a function of atomic size mismatch ($\delta$). Figure 9a shows the $\Omega$ vs $\delta$ plot for the all compositions developed in the diffusion couple. The $\Omega$ varies between 2 and 5, and $\delta$ varies between 0.032 and 0.05. A smaller mismatch ($\delta \leq 0.066$) in atomic size[38,47] and $\Omega \geq 1.1$[47] has been suggested as a criterion for forming a solid solution in HEAs. Figure 9b shows the $\Delta H_{mix}$ vs $\delta$ plot, where the $\Delta H_{mix}$ for FCC $Al_pCo_qCr_rFe_sNi_tMn_u$ compositions was observed to vary from −9 to −4 kJ/mol, which is consistent with the suggested values (−11.6 to 3.2 kJ/mol) reported by Guo et al.[38] Figure 9c shows that the VEC varied between 7.65 and 8.0, which is also consistent with those reported for the single phase FCC solid solution by Poletti and Battezzatti,[50] i.e., VEC > 7.5. However, it contradicted the VEC suggested by Guo et al.[49] at VEC ≥ 8.0. Figure 9d shows that the $\Delta\chi$ varied between 0.072 and 0.08, which is in accordance with the suggested $\Delta\chi \leq 0.175$ for the formation of solid solution,[51] although many exceptions were also documented for this rule.[52]

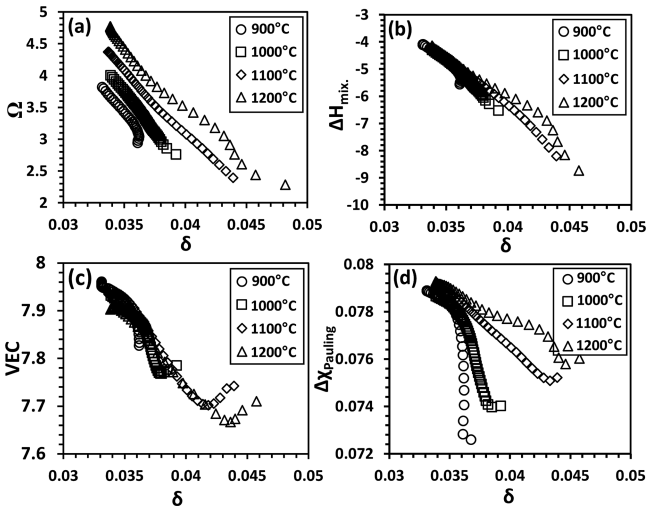


**Figure 9.** Application of solid-solubility predictors to the various off-equiatomic FCC $Al_pCo_qCr_rFe_sNi_tMn_u$ compositions generated in the diffusion couples: (a) $\Omega$–$\delta$, (b) $\Delta H_{mix}$–$\delta$, (c) VEC–$\delta$, and (d) $\Delta\chi$–$\delta$ plots.

## CONCLUSIONS

Off-equiatomic compositions of senary FCC $Al_pCo_qCr_rFe_sNi_tMn_u$ alloys were generated by diffusing Al and Ni into the equiatomic CoCrFeNiMn alloy via solid-to-solid diffusion couples between $\beta$-$Al_{48}Ni_{52}$ (B2) and $Co_{20}Cr_{20}Fe_{20}Ni_{20}Mn_{20}$ (FCC) alloys. The maximum solubility limit for Al in off-equiatomic $Al_pCo_qCr_rFe_sNi_tMn_u$ alloys was determined as a function of temperature and compared to the solubility limit of Al in equiatomic $Al_x$CoCrFeNiMn alloy. At a temperature of 1100 °C and above, off-equiatomic $Al_pCo_qCr_rFe_sNi_t$ alloy exhibited higher Al solubility than equiatomic $Al_x$CoCrFeNiMn alloy. Correspondingly, thermodynamic analyses demonstrated that the off-equiatomic $Al_pCo_qCr_rFe_sNi_tMn_u$ composition with the highest solubility for Al exhibited a higher thermodynamic stability than the equiatomic $Al_x$CoCrFeNiMn alloy. The role of enthalpy was determined to be significant in accomplishing higher thermodynamic stability for the off-equiatomic $Al_pCo_qCr_rFe_sNi_tMn_u$ alloy, since the entropy of mixing is always greater for the equiatomic $Al_x$CoCrFeNiMn alloy composition. Average effective interdiffusion coefficients were determined on either side of the diffusion couples. A comparison of interdiffusion coefficients for constituent elements in the Al−Co−Cr−Fe−Ni−Mn system with relevant lower-order systems suggested that the sluggish diffusion effect is mainly observed in the BCC alloy but not in the FCC alloy. All compositions in off-equiatomic FCC $Al_pCo_qCr_rFe_sNi_tMn_u$ alloys produced within diffusion couples were observed to follow the existing empirical rules for the formation of single phase in HEAs.

## ASSOCIATED CONTENT

### Supporting Information

The Supporting Information is available free of charge at https://pubs.acs.org/doi/10.1021/acscombsci.0c00096.

Average effective interdiffusion coefficients ($\overline{\tilde{D}}_i^{eff}$) of individual elements determined in the present work (Table S1) and comparison of the average effective interdiffusion coefficients ($\overline{\tilde{D}}_i^{eff}$) for Al, Co, Cr, Fe, Ni, and Mn in ternary Fe−Cr−Ni, quaternary Co−Cr−Fe−Ni, quinary Co−Cr−Fe−Ni−Mn, Al−Co−Cr−Fe−Ni, and senary Al−Co−Cr−Fe−Ni−Mn alloys (Table S2 and Table S3) (PDF)



https://dx.doi.org/10.1021/acscombsci.0c00096
ACS Comb. Sci. 2020, 22, 757−767

## AUTHOR INFORMATION


### Corresponding Author

**Abhishek Mehta** − *Advanced Materials Processing and Analysis Center Department of Materials Science and Engineering, University of Central Florida, Orlando, Florida 32816, United States;* orcid.org/0000-0003-0884-856X; Email: abhi@knights.ucf.edu

### Author

**Yongho Sohn** − *Advanced Materials Processing and Analysis Center Department of Materials Science and Engineering, University of Central Florida, Orlando, Florida 32816, United States*

Complete contact information is available at: https://pubs.acs.org/10.1021/acscombsci.0c00096


### Notes

The authors declare no competing financial interest.

## ACKNOWLEDGMENTS

The authors would like to thank Dr. Bharat Gwalani at the Pacific Northwest National Laboratory (PNNL) for providing the pseudobinary phase diagram between Al and equiatomic CoCrFeNiMn alloy, and a valuable technical discussion on HEAs.

## REFERENCES


(1) Yeh, J. W.; Chen, S. K.; Lin, S. J.; Gan, J. Y.; Chin, T. S.; Shun, T. T.; Tsau, C. H.; Chang, S. Y. Nanostructured high-entropy alloys with multiple principal elements: novel alloy design concepts and outcomes. *Adv. Eng. Mater.* **2004**, *6* (5), 299−303.

(2) Cantor, B.; Chang, I.; Knight, P.; Vincent, A. Microstructural development in equiatomic multicomponent alloys. *Mater. Sci. Eng, A* **2004**, *375*, 213−218.

(3) Otto, F.; Yang, Y.; Bei, H.; George, E. P. Relative effects of enthalpy and entropy on the phase stability of equiatomic high-entropy alloys. *Acta Mater.* **2013**, *61* (7), 2628−2638.

(4) Yeh, J. W. Recent progress in high entropy alloys. *Ann. Chim. Sci. Mater.* **2006**, *31* (6), 633−648.

(5) Mehta, A.; Sohn, Y. H. Interdiffusion, Solubility Limit, and Role of Entropy in FCC Al-Co-Cr-Fe−Ni Alloys. *Metall. Mater. Trans. A* **2020**, *51* (6), 3142−3153.

(6) Zhang, F.; Zhang, C.; Chen, S. L.; Zhu, J.; Cao, W. S.; Kattner, U. R. An understanding of high entropy alloys from phase diagram calculations. *CALPHAD: Comput. Coupling Phase Diagrams Thermochem.* **2014**, *45*, 1−10.

(7) Tsai, K. Y.; Tsai, M. H.; Yeh, J. W. Sluggish diffusion in Co−Cr−Fe−Mn−Ni high-entropy alloys. *Acta Mater.* **2013**, *61* (13), 4887−4897.

(8) Vaidya, M.; Trubel, S.; Murty, B. S.; Wilde, G.; Divinski, S. V. Ni tracer diffusion in CoCrFeNi and CoCrFeMnNi high entropy alloys. *J. Alloys Compd.* **2016**, *688*, 994−1001.

(9) Vaidya, M.; Pradeep, K.G.; Murty, B.S.; Wilde, G.; Divinski, S.V. Bulk tracer diffusion in CoCrFeNi and CoCrFeMnNi high entropy alloys. *Acta Mater.* **2018**, *146*, 211−224.

(10) Vaidya, M.; Pradeep, K.; Murty, B. S.; Wilde, G.; Divinski, S. V. Radioactive isotopes reveal a non sluggish kinetics of grain boundary diffusion in high entropy alloys. *Sci. Rep.* **2017**, *7* (1), 12293.

(11) Zhang, C.; Zhang, F.; Jin, K.; Bei, H.; Chen, S.; Cao, W.; Zhu, J.; Lv, D. Understanding of the elemental diffusion behavior in concentrated solid solution alloys. *J. Phase Equilib. Diffus.* **2017**, *38* (4), 434−444.

(12) Gaertner, D.; Abrahams, K.; Kottke, J.; Esin, V. A.; Steinbach, I.; Wilde, G.; Divinski, S. V. Concentration-dependent atomic mobilities in FCC CoCrFeMnNi high-entropy alloys. *Acta Mater.* **2019**, *166*, 357−370.

(13) Kottke, J.; Laurent-Brocq, M.; Fareed, A.; Gaertner, D.; Perrière, L.; Rogal, Ł.; Divinski, S. V.; Wilde, G. Tracer diffusion in the Ni−CoCrFeMn system: Transition from a dilute solid solution to a high entropy alloy. *Scr. Mater.* **2019**, *159*, 94−98.

(14) Gaertner, D.; Kottke, J.; Wilde, G.; Divinski, S. V.; Chumlyakov, Y. Tracer diffusion in single crystalline CoCrFeNi and CoCrFeMnNi high entropy alloys. *J. Mater. Res.* **2018**, *33* (19), 3184−3191.

(15) Dąbrowa, J.; Danielewski, M. State-of-the-Art Diffusion Studies in the High Entropy Alloys. *Metals* **2020**, *10* (3), 347.

(16) Divinski, S. V.; Pokoev, A. V.; Esakkiraja, N.; Paul, A. A mystery of "sluggish diffusion" in high-entropy alloys: the truth or a myth? *Diffusion Foundations (Trans. Technol. Publ.)* **2018**, *17*, 69−104.

(17) Miracle, D.; Senkov, O. A critical review of high entropy alloys and related concepts. *Acta Mater.* **2017**, *122*, 448−511.

(18) Chen, W.; Zhang, L. High-throughput determination of interdiffusion coefficients for Co-Cr-Fe-Mn-Ni high-entropy alloys. *J. Phase Equilib. Diffus.* **2017**, *38* (4), 457−465.

(19) Dąbrowa, J.; Zajusz, M.; Kucza, W.; Cieślak, G.; Berent, K.; Czeppe, T.; Kulik, T.; Danielewski, M. Demystifying the sluggish diffusion effect in high entropy alloys. *J. Alloys Compd.* **2019**, *783*, 193−207.

(20) Mehta, A.; Zhou, L.; Schulz, E. A.; Keiser, D. D.; Cole, J. I.; Sohn, Y. H. Microstructural Characterization of AA6061 Versus AA6061 HIP Bonded Cladding−Cladding Interface. *J. Phase Equilib. Diffus.* **2018**, *39* (2), 246−254.

(21) Park, Y.; Newell, R.; Mehta, A.; Keiser, D. D.; Sohn, Y. H. Interdiffusion and reaction between U and Zr. *J. Nucl. Mater.* **2018**, *502*, 42−50.

(22) Schulz, E. A.; Mehta, A.; Belova, I. V.; Murch, G. E.; Sohn, Y. H. Simultaneous Measurement of Isotope-Free Tracer Diffusion Coefficients and Interdiffusion Coefficients in the Cu-Ni System. *J. Phase Equilib. Diffus.* **2018**, *39* (6), 862−869.

(23) Schulz, E.; Mehta, A.; Park, S. H.; Sohn, Y. H. Effects of Marker Size and Distribution on the Development of Kirkendall Voids, and Coefficients of Interdiffusion and Intrinsic Diffusion. *J. Phase Equilib. Diffus.* **2019**, *40*, 156−169.

(24) Mehta, A.; Dickson, J.; Newell, R.; Keiser, D. D.; Sohn, Y. H. Interdiffusion and reaction between Al and Zr in the temperature range of 425 to 475 °C. *J. Phase Equilib. Diffus.* **2019**, *40* (4), 482−494.

(25) Mehta, A.; Zhou, L.; Keiser, D. D.; Sohn, Y. H. Anomalous growth of $Al_8Mo_3$ phase during interdiffusion and reaction between Al and Mo. *J. Nucl. Mater.* **2020**, *539*, 152337.

(26) He, J.; Liu, W.; Wang, H.; Wu, Y.; Liu, X.; Nieh, T.; Lu, Z. Effects of Al addition on structural evolution and tensile properties of the FeCoNiCrMn high-entropy alloy system. *Acta Mater.* **2014**, *62*, 105−113.

(27) Takeuchi, A.; Inoue, A. Calculations of mixing enthalpy and mismatch entropy for ternary amorphous alloys. *Mater. Trans, JIM* **2000**, *41* (11), 1372−1378.

(28) Bakker, H. *Enthalpies in alloys, Miedema's semi-empirical model*; Enfield Publishing & Distribution Company, 1998.

(29) Takeuchi, A.; Inoue, A. Classification of bulk metallic glasses by atomic size difference, heat of mixing and period of constituent elements and its application to characterization of the main alloying element. *Mater. Trans.* **2005**, *46* (12), 2817−2829.

(30) He, Q.; Ye, Y.; Yang, Y. The configurational entropy of mixing of metastable random solid solution in complex multicomponent alloys. *J. Appl. Phys.* **2016**, *120* (15), 154902.

(31) He, Q.; Ye, Y.; Yang, Y. Formation of Random Solid Solution in Multicomponent Alloys: from Hume-Rothery Rules to Entropic Stabilization. *J. Phase Equilib. Diffus.* **2017**, *38*, 416−425.

(32) Senkov, O.; Miracle, D. A new thermodynamic parameter to predict formation of solid solution or intermetallic phases in high entropy alloys. *J. Alloys Compd.* **2016**, *658*, 603−607.

(33) Liang, S. M.; Schmid-Fetzer, R. Evaluation of Calphad approach and empirical rules on the phase stability of multi-principal element alloys. *J. Phase Equilib. Diffus.* **2017**, *38* (4), 369−381.

(34) Wu, Z.; Bei, H.; Otto, F.; Pharr, G. M.; George, E. P. Recovery, recrystallization, grain growth and phase stability of a family of FCC-structured multi-component equiatomic solid solution alloys. *Intermetallics* **2014**, *46*, 131−140.
(35) Kao, Y. F.; Chen, T. J.; Chen, S. K.; Yeh, J. W. Microstructure and mechanical property of as-cast, -homogenized, and -deformed $Al_xCoCrFeNi$ ($0 \le x \le 2$) high-entropy alloys. *J. Alloys Compd.* **2009**, *488* (1), 57−64.
(36) Wang, W. R.; Wang, W. L.; Wang, S. C.; Tsai, Y. C.; Lai, C. H.; Yeh, J. W. Effects of Al addition on the microstructure and mechanical property of AlxCoCrFeNi high-entropy alloys. *Intermetallics* **2012**, *26*, 44−51.
(37) Wu, B.; Xie, Z.; Huang, J.; Lin, J.; Yang, Y.; Jiang, L.; Huang, J.; Ye, G.; Zhao, C.; Yang, S.; Sa, B. Microstructures and thermodynamic properties of high-entropy alloys CoCrCuFeNi. *Intermetallics* **2018**, *93*, 40−46.
(38) Guo, S.; Hu, Q.; Ng, C.; Liu, C. More than entropy in high-entropy alloys: Forming solid solutions or amorphous phase. *Intermetallics* **2013**, *41*, 96−103.
(39) Tong, C. J.; Chen, Y. L.; Yeh, J. W.; Lin, S. J.; Chen, S. K.; Shun, T. T.; Tsau, C. H.; Chang, S. Y. Microstructure characterization of $Al_xCoCrCuFeNi$ high-entropy alloy system with multiprincipal elements. *Metall. Mater. Trans. A* **2005**, *36* (4), 881−893.
(40) Wang, X.; Zhang, Y.; Qiao, Y.; Chen, G. Novel microstructure and properties of multicomponent $CoCrCuFeNiTi_x$ alloys. *Intermetallics* **2007**, *15* (3), 357−362.
(41) Li, C.; Li, J.; Zhao, M.; Jiang, Q. Effect of alloying elements on microstructure and properties of multiprincipal elements high-entropy alloys. *J. Alloys Compd.* **2009**, *475* (1−2), 752−757.
(42) Wang, W. R.; Wang, W. L.; Yeh, J. W. Phases, microstructure and mechanical properties of $Al_xCoCrFeNi$ high-entropy alloys at elevated temperatures. *J. Alloys Compd.* **2014**, *589*, 143−152.
(43) Dayananda, M. A.; Sohn, Y. H. Average effective interdiffusion coefficients and their applications for isothermal multicomponent diffusion couples. *Scr. Mater.* **1996**, *35* (6), 683−688.
(44) Duh, J. G.; Dayananda, M. A. Interdiffusion in Fe−Ni-Cr Alloys at 1100 °C. *Defect Diffus. Forum* **1991**, *39*, 1−50.
(45) Kulkarni, K.; Chauhan, G. P. S. Investigations of quaternary interdiffusion in a constituent system of high entropy alloys. *AIP Adv.* **2015**, *5* (9), 097162.
(46) Verma, V.; Tripathi, A.; Kulkarni, K. N. On interdiffusion in FeNiCoCrMn high entropy alloy. *J. Phase Equilib. Diffus.* **2017**, *38* (4), 445−456.
(47) Yang, X.; Zhang, Y. Prediction of high-entropy stabilized solid-solution in multi-component alloys. *Mater. Chem. Phys.* **2012**, *132* (2), 233−238.
(48) Fang, S.; Xiao, X.; Xia, L.; Li, W.; Dong, Y. Relationship between the widths of supercooled liquid regions and bond parameters of Mg-based bulk metallic glasses. *J. Non-Cryst. Solids* **2003**, *321* (1), 120−125.
(49) Guo, S.; Ng, C.; Lu, J.; Liu, C. Effect of valence electron concentration on stability of fcc or bcc phase in high entropy alloys. *J. Appl. Phys.* **2011**, *109* (10), 103505.
(50) Poletti, M.; Battezzati, L. Electronic and thermodynamic criteria for the occurrence of high entropy alloys in metallic systems. *Acta Mater.* **2014**, *75*, 297−306.
(51) Yang, X.; Chen, S.; Cotton, J.; Zhang, Y. Phase stability of low-density, multiprincipal component alloys containing aluminum, magnesium, and lithium. *JOM* **2014**, *66* (10), 2009−2020.
(52) Dong, Y.; Lu, Y.; Jiang, L.; Wang, T.; Li, T. Effects of electronegativity on the stability of topologically close-packed phase in high entropy alloys. *Intermetallics* **2014**, *52*, 105−109.


https://dx.doi.org/10.1021/acscombsci.0c00096
*ACS Comb. Sci.* 2020, 22, 757−767